J. Condensed Matter Nucl. Sci. 39 (2025) 165–184

Research Article

Current Status of the Coherent Correlated States for Explanation of LENR

V. I. Vysotskii and M. V. Vysotskyy

Taras Shevchenko National University of Kyiv, Ukraine

Abstract

The study addresses primary issues and paradoxes observed in successful experiments on Low Energy Nuclear Reactions (LENR), including abnormally high probability, significant suppression or absence of radioactive daughter isotopes and accompanying gamma radiation, as well as the stringent selection of specific nuclear reactions. These phenomena cannot be elucidated within the framework of conventional nuclear physics concepts. An analysis of diverse experiments conducted in various material environments and systems such as solids, gases, low-temperature plasma, beams of low-energy particles, biological systems, and astrophysical objects has been performed. The investigation demonstrates that these LENR paradoxes find comprehensive explanations when employing the LENR theory rooted in coherent correlated states of interacting particles.
 ISSN 2227-3123

Keywords: LENR anomalies, Coherent correlated states

1. Introduction

Successful yet paradoxical LENR experiments prompt the quest for suitable theoretical frameworks capable of explaining and optimizing these phenomena. Presently, numerous models, the majority of which predominantly focus on enhancing the tunneling of charged particles, particularly deuterons, at low energies, have been proposed.

However, it's well established that LENR paradoxes extend beyond the remarkably elevated likelihood of LENR at low energy, revealing an equally perplexing and anomalously weak manifestation of accompanying radiative processes. These characteristics bear significant implications for practical applications and offer potential solutions to global environmental challenges posed by traditional nuclear power.

It is evident that a fitting theoretical model should account for all these anomalous effects. Furthermore, for practical optimization of such reactions, it is imperative that the theoretical model rests upon fundamental and well-established principles of nuclear physics and quantum mechanics. The analytical approach to LENR under consideration leverages the application of coherent correlated states, meeting these stringent criteria. The following sections discuss the key prerequisites and potential avenues for realizing such states. Additionally, we provide an overview of the most successful experiments aligning well with this theoretical model.

 ISSN 2227-3123

2. The Fundamental Concept of Implementing LENR Using Coherent Correlated States

To date, numerous successful experiments demonstrating LENR lack a robust theoretical model capable of adequately explaining non-trivial outcomes inconsistent with traditional nuclear physics models. Key challenges in LENR, often deliberated, include:

- the abnormally high probability of overcoming the Coulomb potential barrier during interactions of charged particles with low energy;
- the absence (or very small probability of creation) of radioactive daughter isotopes in observed LENR reactions, an anomaly in the context of conventional nuclear physics;
- a profound suppression (by many orders of magnitude) of gamma radiation, typical in specific nuclear reactions, along with a significant suppression of the neutron channel in the extensively studied (dd)-fusion reaction;
- unusual selectivity in LENR probability and its anomalous inversion during the transition from hot fusion to LENR for different isotopes of certain elements.

Several dozen theoretical models attempt to address these paradoxes based on completely different principles, ranging from super-efficient shielding of atomic nuclei, consideration of quark interaction anisotropy, multibody fusion inside crystalline nano accelerators, "recharging" of protons into neutrons, existence of unknown elementary particles, the presence of super deep "Dirac" levels of electrons in a hydrogen atom etc.

Most studies primarily focus on resolving the first problem concerning the transparency of the barrier. However, it is crucial to address all these challenges simultaneously. For instance, an increase in barrier transparency alone does not explain the prohibition on the formation of daughter radioactive isotopes or the suppression of gamma decay channels. Obviously, such one-sided approach is insufficient. The nontriviality of these unexplained paradoxes can not be ignored, since the lack of an adequate explanation of them is equivalent to the lack of understanding of these processes, and hence the impossibility of their optimization and safe large-scale use.

Moreover, many models concentrate solely on studying one reaction (dd-fusion) in a condensed metal-hydrogen matrix of the PdD type, despite the occurrence of such reactions in diverse environments and systems (in solid, in liquid, in gas, during an electric discharge, in low-temperature plasma, in biological systems, etc.).

In our publications (e.g., [1]–[18]), we explored a comprehensive and universally applicable mechanism for optimizing LENR based on Coherent Correlated States (CCS) of interacting particles.

The fundamental concept revolves around identifying a mechanism that influences interacting particles, increasing the probability of the tunneling effect at low average ambient temperatures, while concurrently elucidating all other LENR paradoxes. Our research demonstrates that achieving this effect is feasible through the utilization of large virtual energy pulses (energy fluctuations) with very short durations.

According to the law of conservation of energy, the action of such a virtual pulse necessitates the rapid occurrence of a nuclear reaction, facilitating a swift release of energy that compensates for the initial energy fluctuation (effectuating the "return of fluctuation energy"). In such a system, the implementation of a reaction channel leading to the formation of daughter radioactive nuclei is precluded. This is because the energy would be "returned" after a prolonged duration, contravening the law of conservation of energy. Correspondingly, gamma radiation in such a system experiences substantial suppression, given its relatively long average generation time.

Coherent correlated states align perfectly with these criteria. They generate extensive energy fluctuations that endure for a relatively prolonged period. This mechanism substantially heightens the probability of LENR and is universally applicable across diverse experiments. Importantly, the CCS method allows the explication of all the aforementioned paradoxes based on the principles of standard quantum mechanics and modern nuclear physics, without resorting to speculative heuristic models.

3. Theoretical and Logical Bases of CCS

In atomic and nuclear physics, the widely used Heisenberg uncertainty relations (1927) address the coordinate and momentum, as well as energy and time:

$$\delta q \delta p \geq \hbar/2, \;\; \delta E \delta t \geq \hbar/2 \tag{1a}$$

and its generalization by Robertson in 1929 for arbitrary dynamical variables A and B:

$$\delta A \delta B \geq | < [\widehat{A}\widehat{B}] > |/2, \delta K = \sqrt{\sigma_K}, \sigma_K =< (\widehat{K} - < K >)^2 >, \tag{1b}$$

In 1930, independently, Schrödinger and Robertson extended these relations to derive a more universal inequality, known as the Schrödinger-Robertson uncertainty relation [19], [20]:

$$\sigma_A \sigma_B \geq | < [\widehat{A}\widehat{B}] > |^2/4(1 - r^2), \tag{2}$$
$$r = \sigma_{\mathrm{AB}}/\sqrt{\sigma_A \sigma_B}, \quad \sigma_{\mathrm{AB}} = (< \widehat{A}\widehat{B} + \widehat{B}\widehat{A} >)/2 - < A >< B >, \quad 0 \leq |r| \leq 1.$$

Here, *r* represents the correlation coefficient between dynamic variables *A* and *B*, indicating the extent of their statistical interdependence and imposing a restriction on the product of the variances.

In specific instances where $A = p, B = q$ or $A = E, B = t$ this relation simplifies to the modified Heisenberg uncertainty relations with the correlation coefficient r:

$$\delta q \delta p \geq \hbar/2\sqrt{1 - r_{\mathrm{pq}}^2} \equiv \hbar^*/2, \hbar^* = G_{\mathrm{pq}}\hbar, \; G_{\mathrm{pq}} = 1/\sqrt{1 - r_{\mathrm{pq}}^2};$$
$$\delta E \delta t \geq \hbar/2\sqrt{1 - r_{\mathrm{Et}}^2} \equiv \hbar^*/2, \hbar^* = G_{\mathrm{Et}}\hbar, \quad G_{\mathrm{Et}} = 1/\sqrt{1 - r_{\mathrm{Et}}^2}. \tag{3}$$

The key distinction between Heisenberg-Robertson and Schrödinger-Robertson uncertainty relations lies in the coefficient of correlation efficiency $G = 1/\sqrt{1 - r^2} \gg 1$. This parameter characterizes the amplification of the fluctuations of dynamic variables *A* and *B*. The significance of *G* is illustrated by a straightforward example that demonstrates the effectiveness of CCS in optimizing nuclear reactions at low energy.

In the case of $A = p, B = q, <q> = 0, <p> = 0$, we can estimate the lower limit (minimum value) of the kinetic energy fluctuation of a particle with mass *M* localized within the spatial interval δq

$$\delta E^{(min)} = (\delta \mathrm{p})^2/2M = G^2\hbar^2/8M(\delta \mathrm{q})^2. \tag{4}$$

Importantly, during the formation of a coherent correlated state, based, for instance, on an excited oscillator, the Schrödinger-Robertson uncertainty relation becomes an evident generalization of (3) and takes the form:

$$(\delta \mathrm{p})^2(\delta \mathrm{q})^2 \geq G^2(2n + 1)\hbar^2/4. \tag{5}$$

In particular, when a proton with a mass M_p is localized in an interatomic region, typical for condensed matter, with $a \approx 1.5$A (in this case, $\delta q \leq 0.75$A), the fluctuation of the kinetic energy of a particle that is in CCS with a large (but realistic) coefficient of correlation efficiency $G \approx 2000$ corresponds to the value $\delta E^{\min} \approx 4\,\mathrm{keV}$. It should be noted that this value formally corresponds to a very low temperature with $n \approx 0$ of the medium in which the given potential well is located. At room temperature, the initial average population of the oscillator levels corresponds to the excitation of the level with $n \approx 5$ and $\delta E^{\min} \approx 40\,\mathrm{keV}$.

A clear and slightly simplified quasi-classical illustration of such a process can be obtained by analyzing the features of the formation of synchronized fluctuations of the kinetic energy of a particle in a one-dimensional parabolic potential well. Each of the *N* eigenfunctions of the particle $\psi_n(q,t)$ in the potential well is characterized by the instantaneous value of the fluctuation of the momentum $\Delta\vec{p}_n(t)$ with the dispersion

$$\sigma_{pn}(t) \equiv (\delta p_n(t))^2 = \left\langle \{\Delta\vec{p}_n(t) - \langle\, \Delta\vec{p}_n(t)\rangle\}^{\;2} \right\rangle = \left\langle [\Delta\vec{p}_n(t)]^2 \right\rangle. \tag{6}$$

In such a system, the mean value $\langle \Delta\vec{p}_n(t)\rangle = 0$ is equal to zero. The formation of the coherent correlated state of the particle leads to phase coincidence and coherent addition (constructive interference) of the momentum fluctuations $\Delta\vec{p}(t) = \sum_n^{N_{\max}} \Delta\vec{p}_n(t)$ for a large number $N_{max} \gg 1$ of different eigenfunctions $\psi_n(q,t)$ forming a superpositional coherent correlated state $\Psi_{\rm corr}(q,r,t)$. A consequence of this interference is the condition $\langle \Delta\vec{p}_n(t)\Delta\vec{p}_m(t)\rangle_{\rm corr} > 0$ that leads to the formation of very large fluctuations of the dispersion of the total momentum of the particle

$$\sigma_{p(corr)} = \left\langle \left\{ \sum_n^{N_{\max}} \Delta\vec{p}_n(t) \right\}^2 \right\rangle_{corr} = \sum_n^{N_{\max}} \sum_{m\neq n}^{N_{\max}} \langle \Delta\vec{p}_n \Delta\vec{p}_m \rangle_{corr} + \sum_n^{N_{\max}} \left\langle (\Delta\vec{p}_n)^2 \right\rangle \approx N_{\max}^2 \langle \Delta\vec{p}_n \Delta\vec{p}_m \rangle_{corr} + N_{\max} \left\langle (\Delta\vec{p}_n)^2 \right\rangle \sim N_{\max}^2 \tag{7}$$

and fluctations of its energy

$$\delta E = \sigma_{p(\rm corr)}/2M. \tag{8}$$

Similar estimates, made using the Schrödinger equation or the density matrix, lead to the same result. It is also crucial to note that, along with the generation of very large fluctuations of momentum and energy in such a correlated state, there is a significant increase in the duration of each of these fluctuations.

One possible method for estimating the influence of the CCS on the tunneling effect and subsequent nuclear transformations is based on considering the formal substitution $\hbar \to \hbar^* \equiv \hbar/\sqrt{1-r^2} \equiv G\hbar$ in the expression for the tunneling probability. Using the example of a particle localized in a parabolic well, it was shown that the direct use of such a substitution in the formula for the tunneling effect probability in the region *L*(*E*) under the barrier near the nucleus with radius *R*

$$D_{r\neq 0} \approx \exp\left\{ -\frac{2\sqrt{1-r^2}}{\hbar} \int_R^{R+L(E)} \sqrt{2M\{V(q)-E\}}\mathrm{dq} \right\} = (D_{r=0})^{\sqrt{1-r^2}} \equiv \sqrt[G]{D_{r=0}} \tag{9}$$

agrees well with the results of an independent rigorous quantum mechanical calculation of the value $D_{r\neq 0}$ under the condition $D_{r=0} \ll 1$.

It is very important that in the limiting case $|r| \to 1$ the transparency coefficient of any potential barrier also increases to the limiting value $P_{|r|\to 1} \to 1$ for any (including very low) energy of the particle or, accordingly, the temperature of the medium where the considered particle is located.

4. Main Methods of CCS Formation

The methods for both CCS calculations and creation in different systems have been thoroughly addressed in [1]–[18], [21]–[24]. The simplest and most adequate method involves analyzing the state of the considered particle in a non-stationary parabolic field, corresponding to a non-stationary harmonic oscillator. In this case, the correlation coefficient can be calculated based on the solution of equations:

$$\frac{d^2\varepsilon}{dt^2} + \omega^2(t)\varepsilon = 0, \varepsilon(0) = 1, \left.\frac{\mathrm{d}\varepsilon}{\mathrm{dt}}\right|_0 = i, \omega(0) = 1;$$
$$r = \mathrm{Re}\left\{\varepsilon^* \frac{\mathrm{d}\varepsilon}{\mathrm{dt}}\right\} \Big/ \left|\varepsilon^* \frac{\mathrm{d}\varepsilon}{\mathrm{dt}}\right|, r^2 = 1 - 1/\left|\varepsilon^* \frac{\mathrm{d}\varepsilon}{\mathrm{dt}}\right|^2; G = 1/\sqrt{1-r^2}. \tag{10}$$

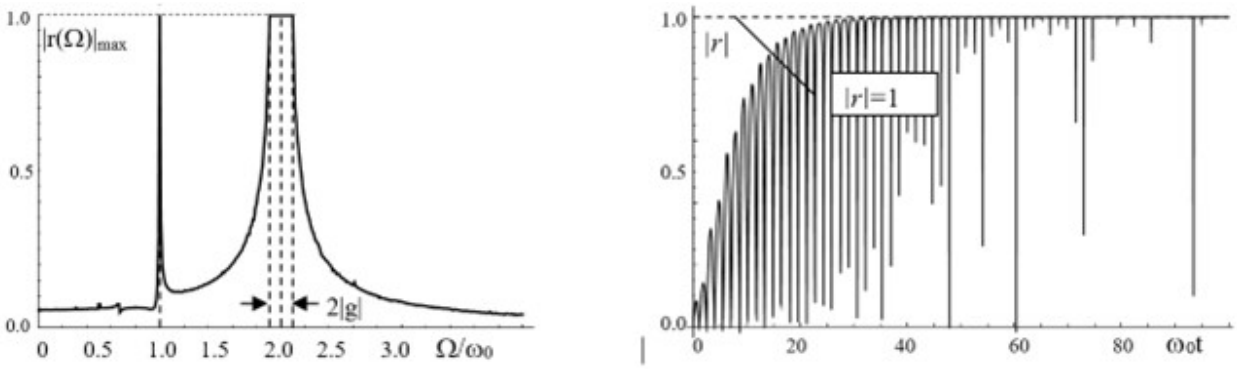

Figure 1. The resonant structure of the dependence of correlation coefficient maximum versus frequency Ω of periodic modulation $\omega(t) = \omega_0(1 + g\cos\Omega t)$(left) and the dependence of the correlation coefficient versus time at $\Omega = 2\omega_0$ and at $g = 0.1$ (right) [5], [6].

Here $\omega(t)$ is the dimensionless frequency normalized to the characteristic oscillator frequency ω_0; t is a dimensionless (normalized to ω_0^{-1}) time; and $\varepsilon(t)$ is the dimensionless (normalized to $q_0 = \sqrt{\hbar/M\omega_0}$) complex coordinate of the particle.

The most effective method of CCS formation is associated with the periodic modulation of the frequency of an equivalent non-stationary harmonic oscillator.

In particular, it was shown that the maximum rate of G increase in the case of harmonic modulation $\omega(t) = 1 + g\cos\Omega t, |g| \ll 1$ (in dimensional form $\omega(t) = \omega_0(1 + g\cos\Omega t)$) corresponds to the condition, when the normalized oscillator modulation frequency Ω is two times greater than the average frequency ω_0 of the oscillator (see Fig. 1).

From these data, it is clear that the most effective mode of CCS formation is the modulation of the parameters of the equivalent oscillator at the parametric resonance frequency $\Omega = 2\omega_0$. Another possible, though less effective mode, corresponds to the modulation of the parameters of an equivalent oscillator at the fundamental frequency ω_0. These highly efficient CCS formation modes can be realized through external modulation of the equivalent oscillator parameters or, for example, with the movement of ions in the channeling mode in a periodic electric field inside the crystal. The effectiveness of other oscillator modulation modes (compression, expansion, pulse change) is determined by the amplitude of the spectral Fourier modulation components at the same frequencies $\Omega = \omega_0$ and $\Omega = 2\omega_0$.

This method can be implemented in different environments and systems. In our works [1]–[18], it was demonstrated that this method of forming a CCS can be implemented in different types of equivalent non-stationary harmonic oscillators (for example, with monotonic expansion or compression, as well as during pulse modulation). Such models can be implemented, for example, in PdD-type targets, where the saturation of the matrix with deuterium leads to the formation of non-stationary microcracks. Similar processes can also occur in growing biological objects, where non-stationary oscillators are formed during cell division (in the space between dividing cells), during DNA division and replication (in the space between separating nucleotides on DNA strands), on the surface of membranes (in places where ions enter membrane channels), and in other locations.

These modes are discussed in detail in [3]–[11], [15]–[18]. In this case, the probability of the formation of a CCS is determined by the amplitude of the spectral component of such modulation at the frequencies $\Omega \approx \omega_0,\ 2\omega_0$ of the fundamental and parametric resonance.

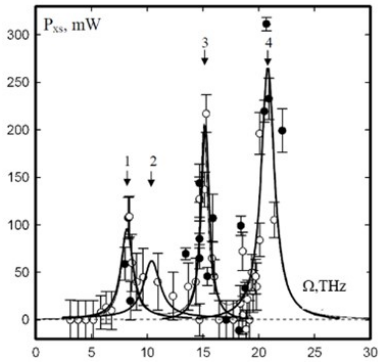

Figure 2. Dependence of the power release generated when a cathode of palladium, saturated with deuterium in a volume of heavy water, is irradiated by difference frequency $|\omega_1 - \omega_2| = \Omega$ from two low-power laser diodes with close frequencies ω_1 and ω_2 [25].

5. Experiments on LENR Stimulation Through Dynamic and Resonant Action on the Active Medium

The results of a theoretical analysis of the LENR stimulation process during resonant modulating action on the active medium align well with known successful LENR experiments. Some of these experiments have been analyzed in [5], [6], [16]–[18], [25]–[33].

5.1. Two-Beam Laser Experiment

This analysis can elucidate the results of the experiments [25] on the stimulation of LENR under the synchronized action of two low-power ($P \leq 20$ mW) laser beams with close frequencies $|\omega_1 - \omega_2| = \Omega \ll \omega_{1,2}$ on the palladium surface of a cathode situated in heavy water in an electrolytic cell, in the presence of an additional external magnetic field. These results are presented in Fig. 2.

When the polarization of these laser beams coincides, the generation of a difference frequency $|\omega_1 - \omega_2| = \Omega$ occurs, acting on the electron concentration in conduction band of the cathode. The action of this low-frequency field leads to the periodic modulation of the potential well parameters for localized deuterium ions in the palladium lattice. By selecting appropriate pairs of such diodes, the authors investigated the dependence of the energy release in such a system on difference frequency in the interval 5–25 *THz* and found four resonance peaks of energy release (Fig. 2) with frequencies $\Omega_1 \approx 7.8{-}8.2$ *THz*, $\Omega_2 \approx 10.2{-}10.8$ *THz*, $\Omega_3 \approx 15.2{-}15.6$ *THz*, and $\Omega_4 \approx 20.2{-}20.8$ *THz*, each having a different amplitude.

Analysis of the deuterium vibrational structure in the palladium matrix shows that the frequencies $\omega_1 \approx 7.8{-}8.2$*THz* and $\omega_2 \approx 10.2{-}10.8$ *THz* correspond to the optical phonon modes (intrinsic vibrations of deuterium ions in the palladium lattice). Each of these ions is, in fact, a harmonic oscillator.

These results align very well with the data of the calculations [11], [12], [15], [16] presented above (Fig. 1, left), assuming that the energy release is connected with the stimulation of nuclear reactions

$$d + d \rightarrow He^3 + n, H^3 + p, He^4; Pd^A + d \rightarrow Ag^{A+2} \rightarrow \cdots \tag{11}$$

at low energy in the volume of palladium saturated with deuterium.

Comparing [16] the dependences of the power output shown on Fig. 2, and, accordingly, the structure of the frequency dependence of the correlation coefficient (Fig. 1, left), it is easy to verify that the first and the third peaks on Fig. 2 correspond to the pair determined by the basic $\Omega = \omega_1 \approx 7.8{-}8.2$ *THz* and parametric $\Omega = 2\omega_1 \approx$

$15.2-15.6$ *THz* frequency resonances of the correlation coefficient formation, and the second and the forth peaks correspond to another pair (basic $\Omega = \omega_1 \approx 10.2-10.8$ *THz* and parametric $\Omega = 2\omega_1 \approx 20.2-20.8$ *THz* frequency resonances).

The ratio of the amplitudes of the maxima of energy release on Fig. 2 fully corresponds to the results presented on Fig. 1, left: the first, lower peak of each pair corresponds to the lower efficiency of the formation of the CCS at the frequency of the main resonance, and the second, higher – to the greater efficiency at the parametric resonance frequency.

The mechanism of CCS formation in this PdD system can be connected with different processes. Most probably, in the PdD compound in "Terahertz" laser experiments [25], such a mechanism can be connected with plasmon excitation and can be based on the following two-step process:

- excitation of the surface electron plasmon and modulation of the electron density on a surface of the PdD compound at a combined action of two coherent laser beams with different frequencies;
- modulation of the frequency of the optical phonon modes of deuterons in elementary cells of the Pd matrix under the action of electron density oscillations in the volume of these elementary cells.

The possibility of the second modulation is connected with the influence of the electron screening on the parameters of the parabolic potential well (e.g., on the depth of the well) in the harmonic oscillators formed by the interaction of the Pd^+ and D^+ ions in the PdD elementary cells.

The presence of an external magnetic field leads to the formation of a nonlinear polarization in the electron plasma of a solid, needed for the generation of the difference frequency at the action of two low-power laser beams with coinciding polarization and small frequency difference. A more detailed analysis of the considered features of this experiment has been carried out in [16].

5.2. Experiment with Cooled Deuterium Gas in a Variable Magnetic Field

Another noteworthy experiment on LENR stimulation [26] was conducted using cooled D_2 gas in a strong variable magnetic field. The schematic representation of the experimental setup and the results of experiments are illustrated in Fig. 3.

The experimental configuration comprised a solenoid (magnetic coil) with high inductance *L* positioned within a vessel, where, in certain instances, liquid nitrogen N_2 was introduced. Within the coil, an ampoule (reactor tube) containing D_2 gas was placed. In the steady-state mode (with a robust electric current of 80 *A* or 100 *A* and magnetic field of 8 kG or 10 kG), the flux of detected neutrons corresponded to the background value $J_n \approx 0.0045\ \mathrm{count}/s$. However, with a rapid change in current within the specified range $80 \leftrightarrow 100$ A (or during the intake of D_2 gas into the reactor tube) and in the presence of cooling, an intense neutron flux $J_n \approx 5\ \mathrm{count}/s$ was recorded for a duration of 3 to 5 seconds (refer to Fig. 3, right).

Using the preliminary calibration data of the neutron detectors in this work [26], it follows that during the magnetic field variation, the neutron channel intensity of nuclear fusion in the cold deuterium gas corresponded to a value of $dN_n/dt \approx (1.3-2) \cdot 10^4$ reactions/s.

Conversely, under similar current switching but in the absence of cooling, neutron emission above the background level was not observed.

As per our analysis [16], these processes align seamlessly with the self-similar formation of CCS and their stimulative impact on the reaction $d + d = He^3 + n$. In such a system, the equivalent oscillator corresponds to the movement of ions in a magnetic field.

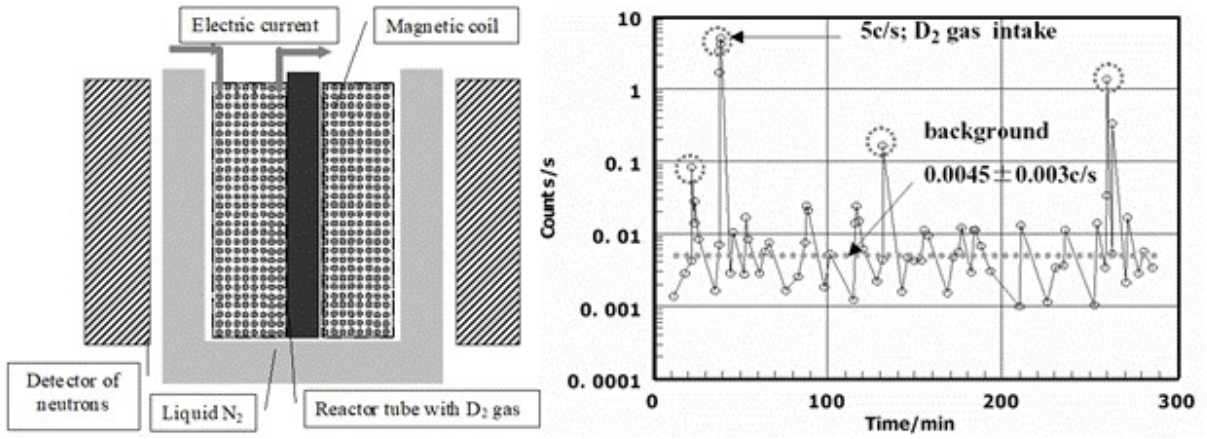

Figure 3. The experimental setup and the dependence of detected neutrons flux versus time in cooled D_2 gas in a strong variable magnetic field [26].

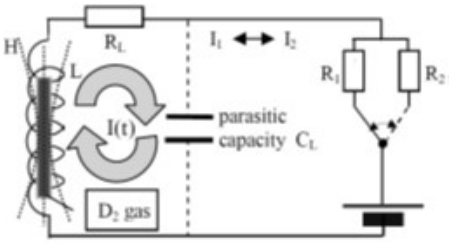

Figure 4. Circuit corresponding to the current switching mode in the experimental setup.

Direct analysis of the employed coil revealed characteristics of inductance $L \approx 10$ H and parasitic (interturn) capacitance $C_L \approx 100$ pF. The natural frequency and reactance of this coil are is equal to

$$\Omega \approx 1/\sqrt{LC_L} \approx 30 \text{ kHz}; \quad X_0 = \sqrt{L/C_L} \approx 300 \text{ k}\Omega. \tag{12}$$

The active resistance of the copper conductor, from which the coil is made, is temperature-dependent and can be expressed as:

$$R_L \approx \begin{cases} 5{-}7\ \Omega\ at\ T = 77K, \\ 70{-}80\ \Omega\ at\ T = 293K, \\ 100{-}120\ \Omega\ at\ T = 373K. \end{cases} \tag{13}$$

From this data, it is evident that the reactance of the circuit significantly exceeds the active resistance and $X_0 \gg R_L$. This ratio corresponds to the periodic mode of oscillation in the equivalent circuit. The presence of inductance, parasitic capacitance, and active resistance leads to the formation of an electric circuit, as depicted in Fig. 4.

In the case of rapid changes in electric current in the outer part of the circuit (due to the fast switching of resistors R_1 and R_2), an oscillating mode of current change occurs:

$$I(t) = I_2 + (I_1 - I_2)\cos(\Omega t)e^{-t/\tau}, \tau \equiv 2L/R_L \gg 2\pi/\Omega. \tag{14}$$

The flow of such an oscillating and slowly decaying electric current results in a similar structure of the magnetic field within the volume of the reactor tube inside the coil:

$$H(t) = H_2 + (H_1 - H_2)\cos(\Omega t)e^{-t/\tau} \equiv H_2[1 + g\cos(\Omega t)e^{-t/\tau}], g = |H_{\max} - H_{\min}|/H_{\max} = 0.2. \quad (15)$$

Direct estimations revealed that during the switch of the current, the stationary values of the magnetic field changed in the interval $H_1 \leftrightarrow H_2 = 8 \leftrightarrow 10$ kOe. The characteristic decay time of current oscillations in the considered oscillatory circuit is determined by the value

$$\tau = 2L/R_L \approx \begin{cases} 3{-}5 \text{ s } at\ T = 77K, \\ 0.3{-}0.2 \text{ s } at\ T = 293K, \\ 0.2{-}0.15 \text{ s } at\ T = 377K. \end{cases} \quad (16)$$

The number of D_2^+ ions in the volume of D_2 gas is always present. The motion of these ions in the presence of a magnetic field corresponds to a harmonic oscillator: it has the same Hamilton operator, the same wave functions $\Psi_n(\xi) = C_n H_n(\xi)e^{-\xi^2/2}$, the same energy spectrum $E_n = (n + 1/2)\hbar\omega_L, n = 1, 2, \ldots$ with a tunable cyclotron frequency

$$\omega_L(t) = \frac{|q|H(t)}{\text{Mc}} \equiv \omega_L(0)[1 + g\cos(\Omega t)e^{-t/\tau}] \approx \omega_L(0)[1 + g\cos\Omega t] \ at\ t < \tau. \quad (17)$$

Here $\omega_L(0) \approx 40$ MHz is the maximum cyclotron frequency at the center of the coil. At the periphery of the coil, the magnetic field decreases sharply. Since the size of the reactor tube significantly exceeded the size of the internal region of the coil, there was different cyclotron frequency amplitude $\omega_L(0)$ in different parts of this tube. The most optimal (with respect to the formation of CCS) frequency ratio $\Omega = 2\omega_L(0)$ corresponded to those ions from the gas composition, which were located at the periphery of the reactor tube

If this condition is met, then the law of frequency change (17) is fully consistent with the condition of CCS formation and, accordingly, allows for effective nuclear fusion.

Another possible mechanism of CCS formation may be associated with the non-resonant low-frequency (at $\Omega \ll \omega_L(0)$) modulation of the parameters of an effective harmonic oscillator [8]. This oscillator corresponds to the state of charged ions in a magnetic field. In the work [8] it has been shown that even with an extremely non-resonant ratio $\Omega \approx (10^{-4} - 10^{-5})\omega_L(0)$, it is possible to form an effective CCS with $G_{\max} \geq 10^3$. The duration of the achievement of such a value $G_{\max}$ is equal to $t_{\text{opt}} \approx (1 - 2)/\Omega \approx (10^4 - 10^5)/\omega_L(0)$ [8]. This result aligns well with the experimental results.

The congruence between the conditions of the real experiment and the theoretical model also allows for an explanation of the unusual influence of the system's temperature on the efficiency of nuclear fusion. Traditionally, nuclear fusion exhibits increased effectiveness with rising temperatures. However, in this experiment, the situation is reversed, and the probability of fusion increases with decreasing temperature.

A rigorous analysis resolves this paradox. At a low temperature $T = 77K$, the resistance of the cooled coil is very small and does not exceed $R_L \approx 7\Omega$. In this scenario, the duration of the oscillatory transient process is prolonged and it is equal to $\tau = 2L/R_L \approx 3{-}5s$. Consequently, during this period, the process of CCS formation can occur, enabling the realization of nuclear fusion.

Conversely, in the opposite scenario (at the absence of forced cooling), the temperature of the coil during the flow of high current can increase to $T \approx 350{-}370K$. This increase results in a sharp rise in the active resistance of the coil and, accordingly, a significant decrease in the duration $\tau = 2L/R_L \approx 0.2s$ of the oscillatory transient process. This reduction poses challenges or even makes it impossible to register reaction products effectively.

In these experiments, a small background neutron flux of 0.0045 pulses per second is observed during the interval between magnetic field switches (see Fig. 3b on the right). This phenomenon may be linked to self-controlled flashing

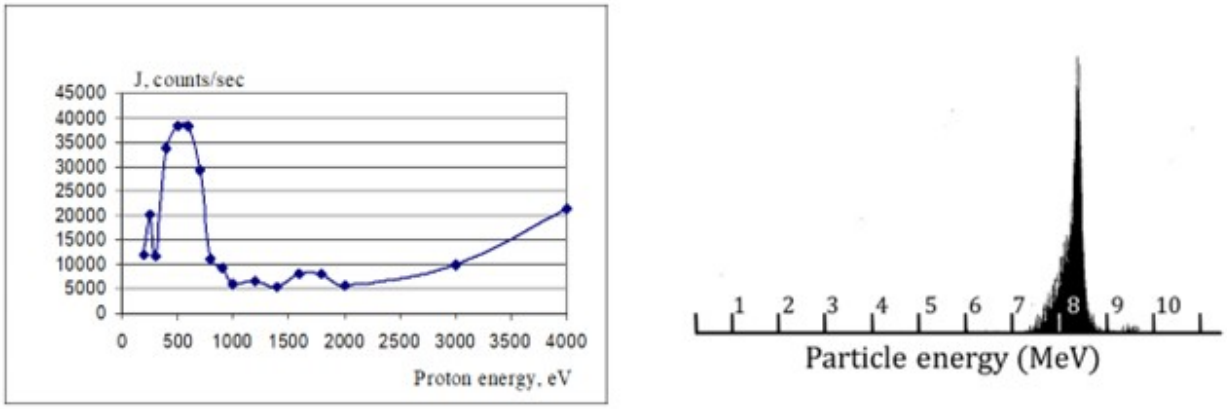

Figure 5. Dependence of the rate of generated fast He^4 nuclei on proton energy (left) and energy spectrum of generated alpha particles He^4 at proton energy $E \approx$ 300–500 *eV* (right) [27].

nuclear fusion occurring within the magnetized weakly ionized D_2 gas [18]. The details of this process are discussed in the following section 4.5.

5.3. Optimization and Anomaly of Accelerator Fusion Using a Low-Energy Proton Beam in a Small-Sized Li Crystal

The analogous mechanism of resonant CCS formation effectively elucidates the anomalous outcomes of experiments involving the implementation of accelerator fusion with a low-energy proton beam [27]. In these experiments, the generation of alpha particles during the interaction of protons with a lithium target (in the form of a solid target or a vapor consisting of *Li* molecular clusters) was investigated with varying kinetic energy of moving protons.

If we analyze this problem based on "traditional" methods of accelerating nuclear $(Li{+}p)$ fusion, one might expect that at low energy, the efficiency of fusion would be minimal until an energy level of about 5–10 *keV*. Afterward, it would monotonously increase up to an energy exceeding 100 *keV*.

However, the actual results of this experiment are strikingly different and are presented in Fig. 5, on the left. It is evident that the nuclear interaction of moving protons with lithium targets is characterized by a sharp peak. The position of this peak corresponds to the energy of particles in a narrow range near $E \approx 500$ *eV*. It can be demonstrated that this result cannot be explained within "standard" models of a nuclear reaction involving accelerated particles. In particular, the direct application of standard formulas of hot fusion to the considered $\mathrm{Li}^7(92.4\%) + p = 2He^4 + 17.3\ \mathrm{MeV}$ reaction yields an extremely small cross section $\sigma(E) \approx 10^{-74} cm^2$, tunneling probability $D(E) \approx 10^{-50}$, and the reaction rate $J < 10^{-58} s^{-1}$. According to these estimations, no fusion reaction should be detected during a particular measurement ($\sim$100 *s*), and, in general terms, not even over the entire duration of the Universe.

On the other hand, the experimental rate of alpha particles in this experiment at resonant energy reached $J_0 \approx 4 \times 10^4 s^{-1}$, which is 10^{62} times more than the expected value.

Another very interesting and surprising aspect of these experiments was the complete absence of alpha particles with energies of 1.9 *MeV* and 2.1 *MeV*, which should be formed in an alternative reaction $\mathrm{Li}^6(7.6\%) + p = He^3(2.3\ \mathrm{MeV}) + He^4(1.7\ \mathrm{MeV})$ with other isotope Li^6 (see Fig. 5, on the right).

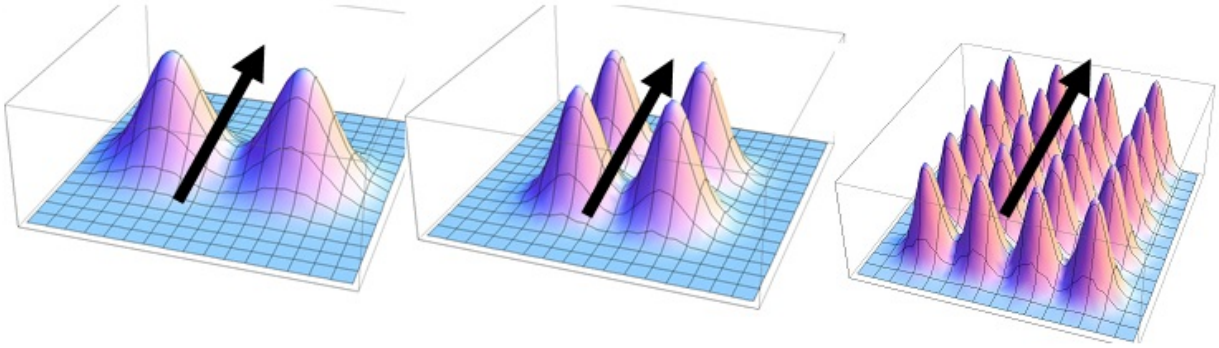

Figure 6. Diagrams of proton motion in the system of potential atom barriers in a diatomic Li_2 molecule, a cluster of two molecules and in a Li crystal.

A crucial observation is that when real (non-virtual) energy is used, the cross section $\sigma(E)$ and astrophysical factor $S(E)$ of this $\mathrm{Li}^6(p, He^3)He^4$ reaction

$$\sigma(E) = \frac{S(E)}{E} \exp\left(-\frac{2\pi Z_1 Z_2 e^2}{\hbar\sqrt{2E/M}}\right), \ \mathrm{S}(E) \approx 4{-}3\ MeV \cdot b \text{ at } E = 10{-}100\ keV\ [28] \tag{18}$$

are 40 times greater than the similar parameters of $\mathrm{Li}^7(p, He^4)He^4$ reaction, for which

$$S(E) \approx 0.1\ MeV \cdot b \text{ at } E = 10{-}100\ keV\ [28]. \tag{19}$$

In works [12], [14]–[15] it was demonstrated that both of these paradoxes can be easily explained if one assume that the fusion reaction in these experiments is facilitated by the formation of a CCS during the passage of a proton through the periodic lithium lattice or through molecules of the lithium vapor (see Fig. 6).

The results of calculation of the change in the correlation coefficient versus distance and the average correlation efficiency coefficient versus proton velocity are presented in Fig. 7. The analysis is based on the fact that the motion of a proton in the system of potential wells and barriers is equivalent to its localization in a nonstationary harmonic oscillator.

From the calculation results, it becomes evident that the maximum value of the correlation coefficient is realized at the optimal velocity, which (considering the lithium lattice parameters) corresponds to the proton energy

$$T_{\mathrm{opt}} = m_p v_{\mathrm{opt}}^2/2 = 2m_p a_z^2 < \omega >^2 \approx 400{-}600\ eV. \tag{20}$$

This alignment is in good agreement with the experimental data.

Another peculiar aspect of these experiments, specifically the absence of the fusion reaction involving the light isotope, is also entirely elucidated by the specificity of the nuclear reactions stimulated by the CCS. These distinctive features will be discussed further below.

5.4. Implementation of LENR Based on the Formation of CCS in Growing Biological Systems

The processes of CCS formation discussed here are also relevant to the realization of LENR and transmutation of isotopes in growing biological objects [29]–[35]. The mechanism for the implementation of such LENR processes

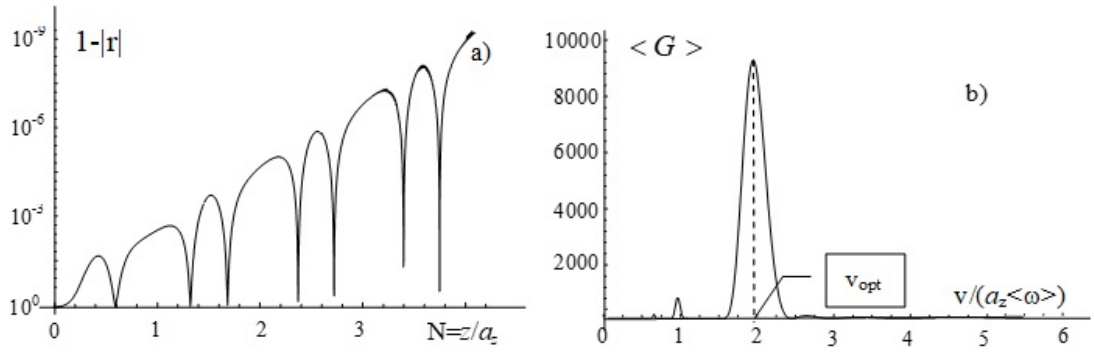

Figure 7. a) The change of the correlation coefficient of a particle moving with the optimal velocity versus distance; b) the average correlation efficiency coefficient <*G*> versus proton velocity.

is associated with rapid topological changes in the microstructure of biological molecules and complexes. These processes are linked to the metabolism of living organisms. In the growth process within living systems, non-stationary microscopic potential wells constantly arise (e.g., during cell division or DNA replication, on membrane surfaces etc.), providing conditions for the formation of CCS and prerequisites for nuclear synthesis.

In our experiments, numerous nuclear reactions

$$Mn^{55} + d = Fe^{57}, Na^{23} + P^{31} = Fe^{54},\ Cs^{133} + p = Ba^{134} \tag{21}$$

were observed in growing biological systems. These reactions were meticulously recorded using precision methods and instruments of nuclear physics, including elemental analysis, mass spectroscopy, Mössbauer spectroscopy, and others.

A highly effective application of such processes relates to the rapid nuclear transformation of radioactive isotopes into stable isotopes of other chemical elements.

In our optimized experiments, the accelerated transmutation reaction $Cs^{137} + p = Ba^{138}$of a long-lived (half-life of 30 years) and hazardous Cs^{137}radioisotope in syntrophic microbiological associations was realized [33]. This process enables the deactivation of an aqueous solution of this isotope by 70% within 10-14 days (Fig. 8).

A further reduction in activity is achievable with additional adjustments in the nutrient composition in the aquatic environment, particularly by incorporating optimal components of the nutrient medium used in the initial stage.

It is noteworthy that the effective implementation of LENR occurs not only in microorganisms but also within the human body. These experiments sought to understand the reasons behind the relatively frequent destruction of titanium implants, commonly utilized the foundation for dentures. Direct experiments demonstrated [34] that the transmutation reaction

$$Ti^{46} + Ca^{48} = Mo^{94} + Q \tag{22}$$

occurs efficiently in the oral cavity, stimulated by microorganisms always present in human saliva.

Even more global processes associated with the stimulation of LENR through biological systems occur at the bottom of seas and oceans [35]. These processes are associated with a fully synchronized change in the isotopic composition of iron found in iron-manganese nodules, with total reserves reaching billions of tons. In all samples recovered from all oceans and seas, an anomalous increase in the concentration of isotopes Fe^{54} and Fe^{56} compared to Fe^{57} was observed. Direct estimates [35] reveal that the overall rate of conversion of $Mn^{55}, P^{31}, \mathrm{Na}^{23}$isotopes

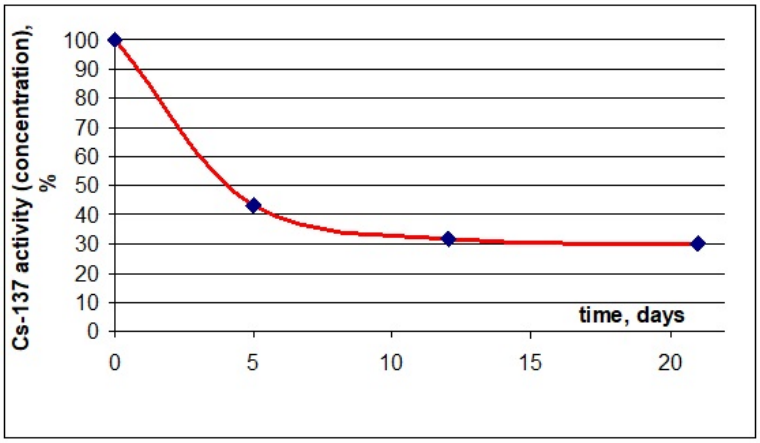

Figure 8. Reduction of gamma-activity of Cs^{137} aqueous solution in the optimized syntrophic microbiological association.

into Fe^{54} and Fe^{56} carried out by microorganisms on the bottom of seas and oceans in reactions $Na^{23} + P^{31} = Fe^{54}$ and $Mn^{55} + p = Fe^{56}$ significantly surpasses the rate of iron production by all metallurgical plants globally. An alternative reaction $Mn^{55} + d = Fe^{57}$ was unlikely due to the very low concentration of deuterium in seawater, which ultimately led to a change in the isotopic composition of iron.

5.5. Self-Controlled Flashing Nuclear Fusion in Stationary Magnetized Low-Temperature Plasma

The prerequisites and mechanism for the implementation of efficient pulsed (flashing) nuclear fusion in a low-temperature stationary hydrogen plasma, with a temperature of $10-20\mathrm{eV}$ in a constant magnetic field, are discussed and investigated in [18].

The characteristics described above of the formation of a CCS and the generation of giant fluctuations in the energy and momentum of a charged particle associated with it can be effectively implemented with a rapid change in the frequency of a nonstationary harmonic oscillator, which corresponds to the movement of a charge in a magnetic field and is characterized by a cyclotron frequency $\omega(t) = qH/\mathrm{mc}$.

At first glance, it might seem that in the case of an oscillator formed on the basis of the interaction of a charge with a constant magnetic field, such an effect can occur only during a short initial time interval immediately after the magnetic field is turned on and has no prospects in stationary systems with a constant magnetic field.

A more detailed analysis reveals that such stationary plasma, in fact, is a dynamic system in which alternating processes of recombination and ionization of atoms and ions occur.

These processes are most pronounced in low-temperature hydrogen plasma with a temperature close to the ionization potential of atoms and exceeding the characteristic potential for the dissociation of hydrogen molecules into atoms.

In such plasma, each act of atom ionization corresponds to a pulsed activation of the interaction of the formed ion with a magnetic field, and each recombination event corresponds to a pulsed deactivation of this interaction.

The duration

$$<t_{\mathrm{ion}}> = S <t_{\mathrm{atom}}> \tag{23}$$

of each interval of the ionic state of hydrogen until the moment of recombination at the plasma temperature $kT_e = 10{-}20\mathrm{eV}$ is much longer than the duration

$$<t_{\mathrm{atom}}> = 1/<\sigma_{\mathrm{ion}} v_e) v_e> n_e \approx <t_{\mathrm{atom}}> \approx (10-1)\cdot 10^8/n_e \ \mathrm{s} \tag{24}$$

of its state in the form of a neutral atom until the moment of ionization.

Here

$$S \approx 4\frac{(m_e kT_e/2)^{3/2}}{\hbar^3 n_{a0}} \exp(-V_i/kT_e) \gg 1 \tag{25}$$

is Saha parameter; $n_e = n_i$ and n_{a0} are, respectively, the concentration of ions and the total concentration of all particles (including neutral atoms) in the plasma.

Each repeated ionization act leads to an automatic rapid activation of the mechanism of quantized motion of the formed ion in a magnetic field H, corresponding to the pulsed excitation of a quantum oscillator with a frequency of $\omega = eH/\mathrm{mc}$. Such a regime immediately leads to the formation of a coherent correlated state of this ion with a correlation coefficient $|r| \to 1$ and to the generation of giant fluctuations in the momentum and kinetic energy $\delta E \geq kT/(1-r^2) \equiv G^2\mathrm{kT}$ of these ions. The amplitude of these fluctuation $kT_i \approx 10{-}20$ eV exceeds the thermal energy of ions by many orders of magnitude [1], [2]. The amplitude of the oscillating value of the coefficient G in such plasma corresponds to the values $G_{\max} \approx 200{-}1000$. At this stage, effective nuclear fusion takes place involving such virtually very "hot" particles and other plasma particles of the corresponding composition (for example, in reactions $(p,d),(d,d),(d,t)$ involving nuclei of hydrogen isotopes). Subsequent triple collisions of these nuclei with electrons in a low-temperature plasma lead to their recombination to the state of neutral atoms. After a short time $<t_{\mathrm{atom}}>$ these atoms are again converted into ions, with the repetition of the considered mechanism of CCS formation and the generation of "hot" ions.

The duration of the process of formation of such states does not exceed $1/\omega_{\mathrm{ion}}$, and the duration of their existence $\Delta t_{\mathrm{ion}}^{(\mathrm{corr})}$ before the decay of the CCS corresponds to several events of ion-ion collisions, the interval between which increases significantly, taking into account the giant fluctuations of the kinetic energy of these ions.

The interconnection and dynamics of these processes are presented schematically in Fig. 9.

It has been demonstrated [18] that the value $\Delta t_{\mathrm{ion}}^{(\mathrm{corr})}$ significantly exceeds the duration $<t_{\mathrm{atom}}>$ of the reverse mode of existence of the considered hydrogen in the form of an atom until the moment of ionization. In this case, the relative (compared to all atoms and heavy ions) fraction of nuclei from the plasma composition, which are at any time in a given system in the CCS and whose state is characterized by anomalously large energy fluctuations, is equal to the efficiency factor for the use of low-temperature plasma for nuclear fusion

$$\eta = P_{\mathrm{diss}} \Delta t_{\mathrm{ion}}^{(\mathrm{corr})}/(<t_{\mathrm{ion}}> + <t_{\mathrm{atom}}>) \approx 0.3{-}0.5. \tag{26}$$

Here P_{diss} is close to 1 probability of dissociation of hydrogen or its isotopes molecules into atoms in the considered range of plasma temperatures $kT \approx (2{-}4)\varepsilon_{\mathrm{diss}}$.

These processes are discussed in detail in [18].

Efficient nuclear fusion on such nuclei in low-temperature plasma at its initial temperature $10{-}20$ eV can last indefinitely long time and does not require much energy.

Another crucial advantage of CCS-based reactions is the possibility of a significant increase in the pulsed effective temperature, which can reach $T_{\mathrm{eff}} \approx G^2 T \approx 100\mathrm{keV}$. This fact allows for reactions between hydrogen and heavier nuclei and, for example, facilitates a promising neutronless reaction $B^{11} + p = 3He^4$.

It is worth noting that such self-controlled nuclear fusion provides an explanation for the phenomenon of anomalously strong heating of the solar atmosphere to $(1{-}2)\cdot 10^6\ K$ at an altitude of several hundred kilometers directly

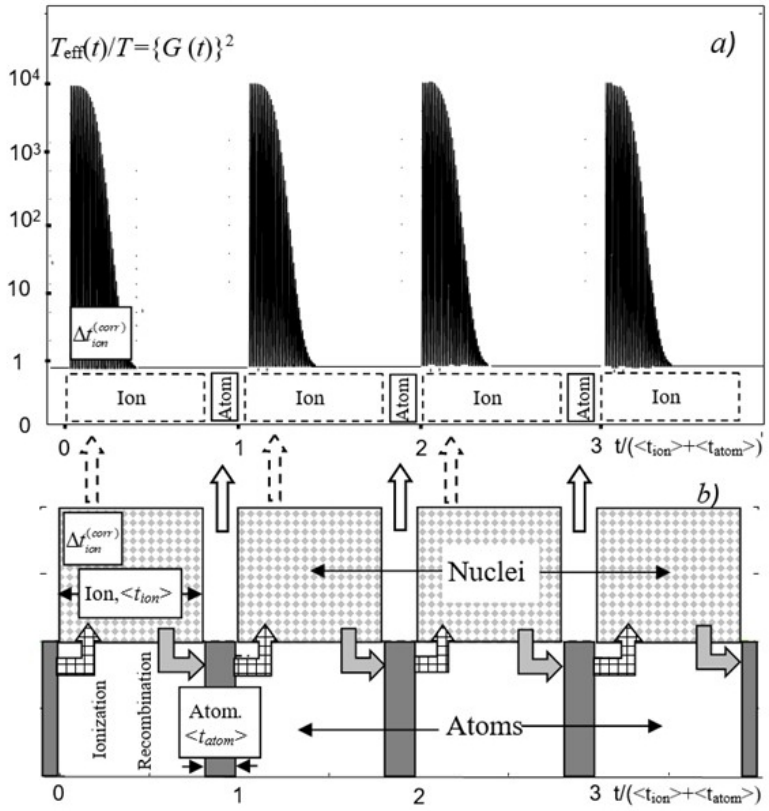

Figure 9. Schematical dynamics of alternating fluctuations of the effective temperature of atoms and ions (*a*) , caused by the alternation of states of ionization and recombination of hydrogen isotopes in low-temperature plasma (*b*).

above its surface, the temperature of which does not exceed 5000 K. Previous multiple unsuccessful attempts to explain these phenomena were often associated with an unrealistic hypothesis about the possibility of "transit" pathways of transferring energy without significant losses from the center of the Sun far beyond its surface through a much colder near-surface medium.

Another mystery is related to the anomalously high concentration of the He^3 isotope relative to He^4 in solar flares and solar cosmic rays compared to the usual $n_{He^3}/n_{He^4} \approx 0.0004$ ratio. The observed increase in this ratio reaches more than 10 times, and this result cannot be explained based on the available data on processes on the Sun.

It is well known from astronomical observations that in this part of the Sun, very frequent vertical ejections of gas-plasma magnetized substance (*spicules*) occur from the volume of the photosphere, stimulated by fast switching (reconnections) of the magnetic field.

At the same time, there are approximately 10^6 such spicules on the Sun, covering about 1% of the Sun's surface. They move with an initial speed of 20–50 *km*/*s*, have a diameter of 500–1200 *km*, an average lifetime of 5–10 minutes, and rise above the chromosphere to the lower part of the solar corona to a height of 6000–10000 *km*. Inside the spicule, there is a longitudinal magnetic field $H_s = 2{-}3$ *kOe*. Some of these spicules leave the solar atmosphere and form streams of cosmic rays that reach the Earth. The typical spicule composition is a weakly ionized "standard" Sun gas

(*H*, *He*, *D*) at an initial temperature of about $T \approx (4{-}5) \cdot 10^3\ K$, with initial atomic $n_{a0} \approx 10^{15}{-}10^{17}\ cm^{-3}$ and ion $n_i \approx 10^{11}{-}10^{13}\ cm^{-3}$ concentrations.

Both of these anomalies (the very strong heating of the solar atmosphere over a relatively cold surface and an excess of He^3 isotope in the composition of cosmic rays) are in good agreement with the mechanism of flashing nuclear fusion in an initially low-temperature magnetized Sun plasma, stimulated by the formation of coherent correlated states in the volume of spicules.

5.6. Suppression of the Radioactive Isotope Creation Channels in Reactions Stimulated by CCS Action

To illustrate the obtained isotope relationships, let's consider the features of the LENR reactions involving protons, Li^6, and Li^7 isotopes [13]. The general schemes of these reactions are the following:

$$Li^6 + p = Be^{7*}\left\{Q = 4\ \mathrm{MeV}, \tau_{\mathrm{reac}} \approx 1.3 \cdot 10^{-13} s\right\} \rightarrow He^3(2.3\ \mathrm{MeV}) + He^4(1.7\ \mathrm{MeV}), \tag{27}$$

$$Li^7 + p = Be^{8*}\left\{Q \approx 17,255\ \mathrm{MeV}, \tau_{\mathrm{reac}} \approx 10^{-20} s\right\} \rightarrow 2He^4 + 17,255\ \mathrm{MeV}. \tag{28}$$

It is necessary to add the time of passage of the particle through the barrier $t_0 \approx (3.3 - 2) \cdot 10^{-20} s$ [13] to the duration of these reactions. Using this value, we find the total duration of both considered nuclear reactions at this energy:

$$(Li^6 p) : \tau_{\mathrm{total}} = \tau_{\mathrm{reac}} + t_0 \approx 1.3 \cdot 10^{-13} s; \tag{29}$$

$$(Li^7 p) : \tau_{\mathrm{total}} = \tau_{\mathrm{reac}} + t_0 \approx (4.3 - 3) \cdot 10^{-20} s. \tag{30}$$

In the "ordinary" uncorrelated state, the probability of the tunneling effect for these reactions at a low temperature of 300–1000 *K* is extremely small and does not exceed $D_{r=0} \approx 10^{-200} - 10^{-100}$.

Let us accept, for a numerical estimate, that for a substantial increase and practical realization of these reactions, the proton has to have kinetic energy not less than $\Delta E \approx 30{-}50$ ***KeV***.

In the case of using the "standard" Heisenberg uncertainty relation $\delta E \delta t \geq \hbar/2$ for uncorrelated states, the kinetic energy fluctuation of $\delta E \approx 30{-}50$ ***keV***, which is necessary for the realization of both reaction, may also exist, but its duration is limited to a very small time interval

$$\delta t_{r=0}^{(\min)} \approx \hbar / 2\delta E \approx (1{-}0.6) \cdot 10^{-20} s, \tag{31}$$

which is clearly insufficient for the implementation of both reactions. This obvious result is due to the fact that the energy fluctuates, spent on overcoming the barrier and forming a compound nucleus, must be returned in a time less than the time allowed by the uncertainty relation. Only under this condition energy fluctuations can stimulate a nuclear reaction.

In the correlated state, with an achievable value $G_{\mathrm{pq}} = 10^3$, the same energy fluctuation $\delta E \approx 30{-}50$ ***keV*** can exist during

$$\delta t_{G_{\mathrm{pq}}=10^3} \approx \hbar G_{\mathrm{pq}} / 2\Delta T \approx (1 - 0.6) \cdot 10^{-17} s. \tag{32}$$

Comparing this value with the total duration $\tau_{\mathrm{total}} \approx (4.3 - 3) \cdot 10^{-20}\ s$ of the reaction (28) $\mathrm{Li}^7 + p = 2He^4$, we can conclude that $\tau_{\mathrm{total}} \ll \delta t_{G_{\mathrm{pq}}=10^3}$ (i.e., the total reaction time is less than the fluctuation lifetime $\delta t_{G_{\mathrm{pq}}=10^3}$, which stimulates this reaction). Thus, such a reaction is consistent with the law of conservation of energy and the corresponding uncertainty relation.

In contrast, for the reaction (27), the opposite condition $\tau_{\mathrm{rtotal}} \gg \delta t_{G_{\mathrm{pq}}=10^3}$ takes place and, therefore, the reaction $\mathrm{Li}^6 + p = He^3 + He^4$ cannot be realized due to the CCS formation process.

These results of the theoretical analysis [12], [14]–[16] fully coincide with the data of detailed experiments of S. Lipinski, H. Lipinski [27], in which low-energy protons interact with a target made of natural lithium. In these

Table 1. Changes in the relative concentrations of lithium isotopes in the Lugano experiment [36].

Isotope	Fuel,%	Ash,%	Natural abundance,%
Li^6	8.6	92.1	7.5
Li^7	91.4	7.9	92.5

experiments, nuclear reactions (28) with the formation of alpha particles He^4 with an energy of about 8.6 *MeV* were observed, but alpha particles He^3 and He^4 with energies of 1.7 *MeV* and 2.3 *MeV*, which correspond to the reaction (27), were completely absent. These experiments were discussed above.

These results also coincide with the data of detailed experiments [36] conducted in 2014 during 32 days in Lugano for the examination of the A. Rossi installation, in which efficient transmutation of Li^7 isotope (characterized by a short reaction time) and complete absence of reactions involving the Li^6 isotope with much longer reaction time, were observed (see Table 1).

We posit that in these experiments the same mechanism of LENR stimulation is implemented as in other analyzed cases - the formation of CCS during the creation and deformation of nanocracks in the volume of metal hydride. The absence of neutrons in these experiments further supports this hypothesis. Similarly, it is evident that this same selection rule prohibits the realization of LENR in reaction channels involving any other isotopes and elements that have a longer reaction time exceeding δt. Considering the smallness of δt even in systems with a large correlation coefficient, reactions passing through the stage of forming long-lived radioactive isotopes fully adhere to this prohibition.

This mechanism also elucidates the strong suppression of gamma radiation in LENR reactions. The majority of gamma transitions in nuclei are characterized by a lifetime $\tau_{\rm rad} \geq 10^{-13}-10^{-14}$ *s* exceeding significantly the duration $\delta t_{G_{\rm pq}\gg 1}$ of the existence of fluctuations for coherent correlated states, resulting in these processes having a very low probability $W_{\rm rad} \approx \delta t_{G_{\rm pq}\gg 1}/\tau_{\rm rad}$.

It should also be noted that the same patterns distinguish the features of any reactions utilizing virtual energy in the form of short-term fluctuations of large amplitude from reactions stimulated by particles with real energy with the same amplitude. The primary distinctions are associated with the prohibition of both the implementation of any endoenergetic reactions and reactions with the formation of a long-lived intermediate nuclear state with a lifetime $\tau_{\rm rad} \gg \delta t$.

In conclusion, it should be noted that, under certain conditions, radioactive daughter nuclei can be formed in such reactions. To achieve this, the reaction must consist of two stages, the first of which will be very short (less than $\delta t \approx G\hbar/2\delta$E) and will be accompanied by the release of energy exceeding the fluctuation energy δE necessary to implement this reaction. In this case, during the second stage, the formation of a daughter radioactive isotope is possible. This situation is realized, in particular, in the reaction $d + d = H^3 + p$, which leads to the formation of tritium [37].

6. Summary

The analysis demonstrates that the utilization of coherent correlated states provides a straightforward and logically consistent solution to the entire complex of fundamental challenges associated with the validation and enhancement of key features in LENR. An important and interesting observation is that the specificity of the manifestation of such states (the combination of an anomalously large amplitude of energy oscillations and a short, controlled duration of their existence) facilitates the resolution of problems that traditional nuclear physics, relying on real (not virtual) particle energy, fundamentally struggles to address. Among these significant issues are the possibility to suppress

nuclear reaction channels leading to the formation of radioactive daughter nuclei and the substantial attenuation of the accompanying gamma radiation. The undoubted relevance of such reactions is self-evident.

The foundational theoretical aspect of these studies closely aligns with our previous analysis of methods to control gamma decay and techniques to influence radiation processes related to cavitation phenomena (e.g., [38], [39]).

It should be noted that above-discussed features of the formation and application of Coherent Correlated States (CCS) for particles such as protons or deuterons are based on the model of their confinement in a non-stationary parabolic potential, corresponding to a non-stationary harmonic oscillator. Crucially, for reactions involving two implanted deuterons or the interaction between a deuteron and another nucleus located in neighboring crystalline cells, the formation of the CCS is required for only one of the deuterons.

A complete equivalence with the harmonic oscillator model is achieved when a charged particle is subjected to a magnetic field, as occurs in nuclear fusion within a stationary magnetized low-temperature plasma [18], [40] or in cooled D_2 gas in a strong variable magnetic field [26].

The formation of CCS for a light particle located in a solid matrix or biological system composed of heavier atoms takes place when the particle is localized within a potential well formed by neighboring heavy atoms. The central part of such a potential typically corresponds to a parabolic potential well, which can occupy a significant portion of the interatomic space. The specific features of CCS formation, considering the deviations between the non-central part of the real interatomic potential well and the ideal parabolic potential, will be examined in future work.

References

[1] V. I. Vysotskii, S.V. Adamenko. Correlated states of interacting particles and problems of the Coulomb barrier transparency at low energies in nonstationary systems. *J. Technical Physics*, **55**(5) (2010) 613.

[2] V. I. Vysotskii, M. V. Vysotskyy, S. V. Adamenko. Formation and application of correlated states in non-stationary systems at low energy of interacting particles. *J. Exp. Theor. Phys.(JETP)*, **114**(2) (2012) 243.

[3] V. I. Vysotskii, S. V. Adamenko, M. V. Vysotskyy. The formation of correlated states and the increase in barrier transparency at a low particle energy in nonstationary systems with damping and fluctuations. *J. Exp. Theor. Phys.(JETP)*, **115**(4) (2012) 551.

[4] V. I. Vysotskii, S. V. Adamenko, M. V. Vysotskyy. Subbarier interaction of channeling particles under the self-similar excitation correlated states in periodically deformed crystal. Jour. of surface investigation, **6**(2) (2012) 369.

[5] V. I. Vysotskii, M. V. Vysotskyy. Coherent correlated states and low-energy nuclear reactions in non stationary systems. *European Phys. Journal* A**49** (2013), issue 8:99, p.1–12.

[6] V. I. Vysotskii, S. V. Adamenko, M. V. Vysotskyy. Acceleration of low energy nuclear reactions by formation of correlated states of interacting particles in dynamical systems. *Annals of Nuclear energy*, **62** (2013) 618.

[7] V. I. Vysotskii, M. V. Vysotskyy. Correlated states and transparency of a barrier for low-energy particles at monotonic deformation of a potential well with dissipation and a stochastic force. *J. Exp. Theor. Phys. (JETP)*, **118**(4) (2014) 534.

[8] V. I. Vysotskii, M. V. Vysotskyy. Formation of correlated states and optimization of nuclear reactions for low-energy particles at nonresonant low-frequency modulation of a potential well. *J. Exp. Theor. Phys. (JETP)*, **120**(2) (2015) 246.

[9] V. I. Vysotskii, M. V. Vysotskyy. The formation of correlated states and optimization of the tunnel effect for low-energy particles under nonmonochromatic and pulsed action on a potential barrier. *J. Exp. Theor. Phys. (JETP)*, **121**(4) (2015) 559.

[10] V. I. Vysotskii, M. V. Vysotskyy. Coherent correlated states of interacting particles – the possible key to paradoxes and features of LENR. *Current Science*, **108**(4) (2015) 30.

[11] V. I. Vysotskii, M. V. Vysotskyy. The formation of correlated states and tunneling at low energy at controlled pulse action on particles. *J. Exp. Theor. Phys. (JETP)*, **152**(8) (2017) 234.

[12] V. I. Vysotskii, M. V. Vysotskyy., S. Bartalucci. Features of the formation of correlated coherent states and nuclear fusion induced by the interaction of slow particles with crystals and free molecules. *J. Exp. Theor. Phys.(JETP)*, **127**(3) (2018), 479–490.

[13] V. I. Vysotskii, M. V. Vysotskyy. Peculiarities of correlated states and the mechanism of automodeline selection of nuclear reaction channels with low energy of charged particles. *J. Exp. Theor. Phys.(JETP)*, **128** (6), (2019), 856–864.

[14] S. Bartalucci, V. I. Vysotskii, M. V. Vysotskyy, Correlated states and nuclear reactions: An experimental test with low energy beams. *Phys. Rev. Accelerators and Beams*, **22**,(2019) # 5, 054503.
[15] V. I. Vysotskii, M. V. Vysotskyy, S. Bartalucci. Using the method of coherent correlated states for production of nuclear interaction of slow particles with crystals and molecules. *Jour. of Condensed Matter Nucl. Sci*. **29** (2019), 358–367.
[16] V. I. Vysotskii, M. V. Vysotskyy. Universal mechanism of LENR in physical and biological systems on the base of coherent correlated states of interacting particles. Cold Fusion. Advances in Condensed Matter Nuclear Science, Edited by Jean-Paul Biberian. Elsevier, 2020. CHAPTER 17, pp. 333–370
[17] V. I. Vysotskii, M. V. Vysotskyy. Application of Correlated wave Packets for Stimulation of LENR in Remote Targets. *Jour. of Condensed Matter Nucl. Sci*., **33** (2020), 305–313.
[18] V. I. Vysotskii, M. V. Vysotskyy. Self-controlled flashing nuclear fusion in stationary magnetized low-temperature plasma. *Fusion science and technology*, **79**:5 (2022), 537–552.
[19] E. Schrödinger. Heisenbergschen Unschärfeprinzip. *Ber. Kgl. Akad. Wiss.,* Berlin, S24 (1930) 296.
[20] H. P. Robertson. A general formulation of the uncertainty principle and its classical interpretation, *Phys.Rev.* **35**A (1930) 667.
[21] V. V. Dodonov, E. V. Kurmishev, V. I. Manko. Generalized uncertainty relation and correlated coherent states, *Phys. Lett*. A**79** (1980) 150.
[22] V. V. Dodonov, A. B. Klimov, V. I. Manko. Low energy wave packet tunneling from a parabolic potential well through a high potential barrier, *Phys. Lett*. A **220** (1996) 41.
[23] V. V. Dodonov, V. I. Manko. "Invariants and correlated states of nonstationary systems", in: Invariants and the Evolution of Nonstationary Quantum Systems, Nova Science, Commack, New York, v.183 (1988) 103–261.
[24] V. V. Dodonov, K. A. B. Limov, V. I. Manko. Physical effects in correlated quantum states", in: Squeezed and Correlated States of Quantum Systems, Nova Science, Commack, New York, v.**295** (1993) 61–107.
[25] D. Letts, D. Cravens, P. Hagelstein. Low-Energy Nuclear Reactions Sourcebook. American Chemical Society, Washington DC, 2009, 2:81–93.
[26] T. Mizuno, T. Akimoto, A. Takahashi, F. Celani. Neutron emission from D2 gas in magnetic fields under low temperature //Condensed Matter Nuclear Science, Proceed. of 11th ICCF Conference, Marseilles, France, 31 Oct. – 5 Nov. 2004, World Scientific, Singapore, 2006, 312–323.
[27] S. Lipinski, H. Lipinski. Hydrogen-lithium fusion device, Intern. patent WO 2014/189799 A9.
[28] C. Angulo, M. Arnould et al. A compilation of charged-particle induced thermonuclear reaction rates, *Nuclear Physics* A **656** (1999), 3–183.
[29] V. I. Vysotskii, A. A. Kornilova. Nuclear fusion and transmutation of isotopes in biological systems, Monograph, Publishing House "Mir", 2003, 302 p.
[30] V. I. Vysotskii, A. A. Kornilova. Nuclear transmutation of stable and radioactive isotopes in biological systems. Book, Pentagon Press, India, 2010, 187 p.
[31] V. I. Vysotskii, A. A. Kornilova. Transmutation of stable isotopes and deactivation of radioactive waste in growing biological systems. *Annals of Nuclear Energy*, **62** (2013) 626–633.
[32] V. I. Vysotskii, A. A. Kornilova. Microbial transmutation of Cs-137 and LENR in growing biological systems. *Current Science*, **108** (2015) 142.
[33] V. I. Vysotskii, A. A. Kornilova. Effective LENR and transmutation of stable and radioactive isotopes in growing biological systems. Cold Fusion. Advances in Condensed Matter Nuclear Science, Edited by Jean-Paul Biberian. Elsevier, 2020. CHAPTER 12, pp. 205–232.
[34] A. A. Kornilova, S. N. Gaydamaka, A. I. Panchishin, V. I. Vysotskii, M. V. Vysotskyy, A. A. Bolotokov. The possible role of LENR in dentistry. *Jour. of Condensed Matter Nucl. Sci*., **33** (2020), 333–339.
[35] V. I. Vysotskii, A. A. Kornilova, S. N. Gaydamaka, A. A. Novakova D. S. Novikov, M. V. Vysotskyy, V. V. Avdonin. Creation of Fe isotopes in natural geology crusts as the result of self-controlled global biostimulated LENR in oceans and seas. *Jour. of Condensed Matter Nucl. Sci*., **33** (2020), 323–332.
[36] G. Levi, E.Foschi, B. Höistad, R. Pettersson, L. Tegnér, H. Essén. Observation of abundant heat production from a reactor device and of isotopic changes in the fuel, Official expertise in Lugano, 2014; http://www.sifferkoll.se/sifferkoll/wp-content/uploads/2014/10/LuganoReportSubmit.pdf.

[37] V. I. Vysotskii, A. A. Kornilova. Generation of microwave self-channeling undamped temperature waves and their application for stimulating nuclear fusion in remote and behind-screen targets. *Nuclear Inst. and Methods in Physics Research, A*, 1058 (2024) 168823.

[38] A. A. Kornilova, V. I. Vysotskii etc. Generation of intense X-rays during ejection of a fast water jet from a metal channel to atmosphere. *Journal of Surface Investigation*, **4**(6) (2010), 1008–1017.

[39] V. I. Vysotskii, V. P. Bugrov, A. A. Kornilova, R. N. Kuz'min, S. I. Reiman. The problem of gamma-laser and controlling of Mössbauer nuclei decay (theory and practice). *Hyperfine Interactions*, **107**(1-4) (1997), 277–281.

[40] V. I. Vysotskii, M. V. Vysotskyy. Mechanism and dynamics of quasi-stationary self-supporting LENR in low-temperature magnetized plasma. *Jour. of Condensed Matter Nucl. Sci*., **38** (2024), 326–337.